Available online at www.sciencedirect.com
ScienceDirect
Earth and Planetary Science Letters 251 (2006) 179–198
EPSL
www.elsevier.com/locate/epsl

Late Mesozoic volcanism in the Great Xing'an Range (NE China): Timing and implications for the dynamic setting of NE Asia

Fei Wang *, Xin-Hua Zhou, Lian-Chang Zhang, Ji-Feng Ying, Yu-Tao Zhang, Fu-Yuan Wu, Ri-Xiang Zhu

State Key Laboratory of Lithospheric Evolution, Institute of Geology and Geophysics, Chinese Academy of Sciences, Beijing 100029, China

Received 23 February 2006; received in revised form 5 September 2006; accepted 5 September 2006
Available online 11 October 2006
Editor: Scott King

Abstract

Mesozoic volcanism is widespread throughout northeastern China, but precise geochronological constraints were previously lacking. Twenty samples, including basalt and basaltic andesites, from the Great Xing'an Range were collected and subjected to $^{40}Ar/^{39}Ar$ dating. The ages mainly concentrate in four periods: ~163–~160 Ma, ~147–~140 Ma, ~125–~120 Ma and ~116–~113 Ma, show that the volcanic succession pulsed from ~160 Ma in the Late Jurassic until the Early Cretaceous. This result, combined with the previous compilation of data from the adjacent areas, suggest a volcanic migration from west to east in the northeastern Asia. These volcanic rocks were formed in an extensional setting, as indicated by the occurrence of A-type granites, mafic dyke swarms, metamorphosed core complexes and basins. The timing (~160–140 Ma) of mantal underplating and transition from crustal contraction to extension in this region suggests that all these geological activities occurred immediately followed the closure of Mongol–Okhotsk ocean, which supposed to be closed by ~160 Ma. Based on these observations, a shears-shaped lithospheric delamination mechanism is proposed to construe the geodynamic scenario of northeastern Asia during Late Mesozoic: the collision between north China and Siberia around ~160 Ma obstructed the westwards movement of the lithosphere induced by the subduction of Pacific plate, this tremendous stress caused the thickened lithospheric delaminating from west edge of the northeast China–Mongolia block at ~160 Ma and extended gradually eastwards. This led to mantle upwelling and underplating, resulting volcanism migration from west to east in northeastern Asia during Late Mesozoic.
© 2006 Elsevier B.V. All rights reserved.

Keywords: volcanism; $^{40}Ar/^{39}Ar$ dating; NE Asia; dynamic setting

1. Introduction

Late Mesozoic volcanic rocks occur over a vast area in northeastern China (NEC) and its adjacent areas — eastern and southern Mongolia, Korean Peninsula, and Japan (Fig. 1). Many geological, petrological and chronological studies were carried out on these magmatic activities [1–6], which have not resulted in a consensus about the mechanism. For instance, a mantle plume hypothesis has been proposed to interpret this extensive Late Mesozoic magmatism in the Great Xing'an Range [7,8]; Fan et al. [5] attributed this magmatic event to post-orogenic diffuse extension after the closure of the paleo-Asia and /or Mongol–Okhotsk

* Corresponding author. Institute of Geology and Geophysics, Chinese Academy of Sciences, Beijing 100029, China. Tel.: +86 10 62007357; fax: +86 10 62028617.
E-mail addresses: wangfei@mail.iggcas.ac.cn, wfdzs@263.net (F. Wang).

0012-821X/$ - see front matter © 2006 Elsevier B.V. All rights reserved.
doi:10.1016/j.epsl.2006.09.007

Oceans; mantle delamination was supposed to be the mechanism of the significant magmatism in the NEC [6].

It was noted that, largely based on the K–Ar ages, the igneous rocks turn younger in age oceanwards along the Asia continental margin [2–4], but its mechanism was also in dispute. Ridges subduction of Kula-pacific plate was proposed for this migration of igneous activities by Kinoshita [2,3], whereas Zhou and Li [4] argued that as the slab dip angle increased, the simple subduction of the Kula-pacific could explain the migration of magmatic activity along southeast China coastal line.

Lacking of precise geochronological data on these volcanics, especially on the basalts, causes the disputes and hampers the advancing in the study on the mechanism of magmatism in NEC. Recently, an igneous event ranging from 120 to 130 Ma in northeastern China was found based on the summary of the dates on plutons [6]. However, these are still indirect age constraints from the intrusive rocks whose exact time relation with the volcanics eruption is unknown. More importantly, precise dating directly on the volcanic successions in the Great Xing'an Range is hence highly desirable, which is crucial to understand the relation between NEC and Mongol–Okhotsk suture zone. In this paper, results of $^{40}Ar/^{39}Ar$ dating of the volcanic rocks in the Great Xing'an Range are presented. In conjunction with the previous compilations of dating results in the adjacent areas, including southern and eastern Mongolia [9,10], northeast China [6,9,11], Korean Peninsula and southwest Japan [2], the temporal-spatial distribution is established. This is potentially a powerful tool that can be used to decipher tectonic mechanisms of the region during the Late Mesozoic. As a conclusion, a new model is suggested attempting to explain this temporal-spatial distribution of volcanism in a frame of plate tectonics.

2. Some basic observations

In the following, we will summarize and comment on some basic observations on Late Mesozoic volcanic rocks and geological settings in NEC:

(1) Late Mesozoic volcanic rocks in NEC cover ~100,000 km^2 in the Great Xing'an Range [12], with cumulative thickness of the successions is up to ~4–5 km [13,14]. These rocks comprise a wide spectrum of rock types, including basalts, basaltic andesite, trachyte, rhyolite, volcanic clastic and tuff. Based on the lithological associations and lava flow sequence, three group divisions in this region are widely accepted: a) The Tamulan

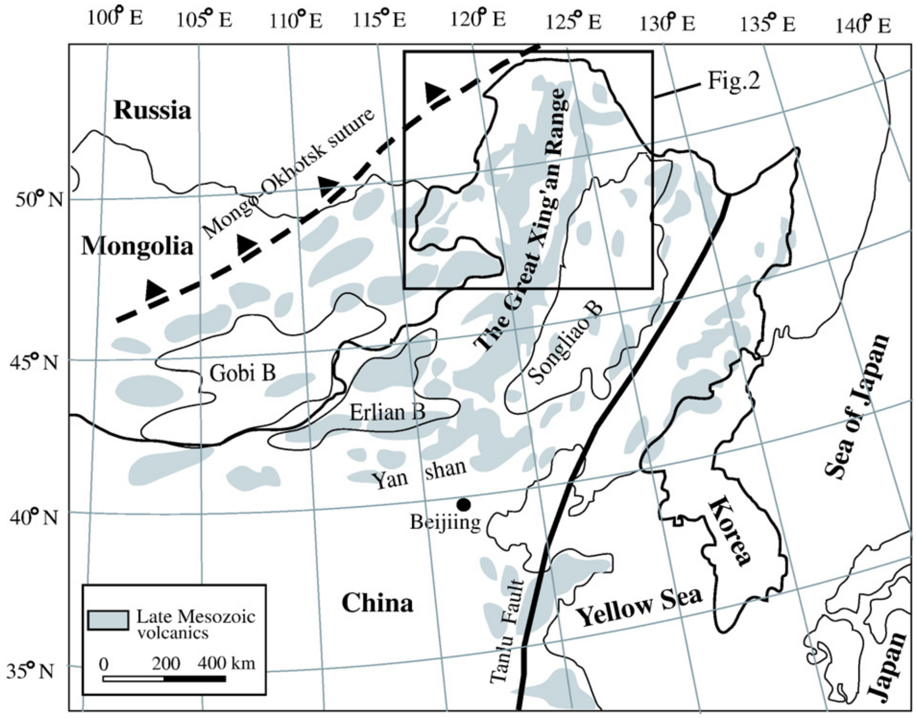

Fig. 1. Geological setting, volcanics distribution of Northeastern China and its adjacent areas. Modified from Meng [9].

formation, the base of the volcanic sequence, is composed mainly of basalts and basaltic andesites. These are commonly subaphyric to weakly porphyritic with predominant phencrysts of pyroxene of 1–3 mm with rare olivine and plagioclase. The matrix is mainly composed of fine-grained or aphanitic clinopyroxene and plagioclase (<0.2 mm) and a few opaque oxides. b) The Shangkuli formation, the most widespread one, exhibits columnar joints and is comprised mainly of basaltic andesite, trachyte, minor pyroclastic tuff and subparallel layers with tuffecous sandstone interbeddings in rhyolitic lavas. These rocks generally show a porphyritic fabric with phenocrysts of plagioclase and hornblende of 4–7 mm grain size. The matrix includes fine-grained plagioclase and hornblende of 0.2–0.5 mm and few opaque oxides. c) The Yiliekede formation is composed mainly of basalts and andesitic basalts. These are subaphyric to weakly porphyritic with dominant phenocrysts of pyroxene of 1–3 mm with rare olivine and plagioclase. The matrix is mainly composed of fine-grained or aphanitic clinopyroxene and plagioclase (<0.2 mm) and opaque oxides are few. In order to constrain the magmatism from the upper mantle, our works mainly focused on the lavas of basalts and basaltic andesites.

(2) The volcanic rocks also occur in the other parts of NEC, including Songliao Basin, Jiaodong peninsular, Yanshan and Liaoxi area. In the south and east of Mongolia along its border with China, volcanics are also the dominant rock, such as in Gobi Basin [10]. The distribution of these volcanics are constrained by the tectonic lines parallel to both the Mongol–Okhotsk suture and Pacific plate suduction zone (Fig. 1).

(3) They exhibit very similar initial Sr (0.704–0.706) and Nd (εNd(t): −0.78–+1.26) isotopic ratios despite their lithological differences [5], and significant LILE, LREE enrichment and strong Nb–Ta depletion. This slightly enriched Sr and weakly depleted to slightly enriched Nd isotopic ratios and enrichment of incompatible elements seem to favor a lithospheric mantle rather than depleted mantle reservoirs in their origin [5,15,16]. Granitic plutonism also companied eruption of the volcanic rocks in NEC in Late Mesozoic time. Plutons are mainly alkali and perakaline and geochemically resemble the volcanics, with ratios of initial ^{87}Sr/^{86}Sr (~0.705) but high positive value of εNd(t) (~+2.5), implying considerable mixing of mantle and crustal materials [17].

(4) Extensional structures reworked the NEC during Late Mesozoic time. Basins began developing, such as Erlian, Hailar, Songliao basins and eastern Gobi basin in southeastern Mongolia. In eastern Gobi basin across the boarder of eastern Mongolia and China, a volcanic interlayer at the lower part of basin boreholes yield a ^{40}Ar/^{39}Ar age of 155 ±1 Ma [18]. Although there are no date on the cored volcanic rocks in the Erlian basin, equivalents of the Xinganling Group in outcrops in West Liaoning are well constrained by ^{40}Ar/^{39}Ar and K–Ar from ~156 Ma [9]. Volcanism started in Songliao basin at Late Jurassic basted on the ^{40}Ar/^{39}Ar and K–Ar ages 157.9±2.7 Ma on a basalt at the base of a drill [11]. These dates suggests that the basins in NEC began rifting at ~155 Ma synchronously.

(5) Topographically, there is a sharp altitude contrast in NEC between the high plateaus to the west and hilly plains to the east along the Great Xing'an Range. The Great Xing'an Range, which represents the steepest altitude gradient from the east to west of NEC, also coincides with the steepest gradient in gravity anomalies and crustal thickness [19]. Interestingly, it also marks the steepest gradient in mantle seismic velocity clearly seen at depths of 100 km and 150 km [19]. The sudden seismic velocity decrease across the Great Xing'an Range from the west to the east is consistent with the interpretation that at such depths the mantle beneath the plateaus in the west is "cold" and "fast" lithosphere whereas beneath the east it is the "hot" and "slow" asthenosphere. The latter is consistent with the recognition that the lithosphere beneath eastern China, including NEC, is anomalously thin, considering the geologically perceived cratonic nature in the North China. Petrologically, the existence of Paleozoic diamondiferous kimberlites in the NEC (e.g., Fuxian in Liaoning Province, Mengyin in Shandong Province) [20–23], all indicates that the NEC lithosphere must have been ~200 km thick back in the Paleozoic. However, recent studies of mantle xenoliths [24–29] indicate a much thinner present-day lithosphere, perhaps no more than 80 km thick beneath NEC. This is confirmed both by seismic studies [30] and mantle tomography [19]. Hence, the lithosphere beneath NEC must have lost 120 km thick bottom portion [31], probably in the Mesozoic [23,29,31–37].

3. The $^{40}Ar/^{39}Ar$ dating techniques

Twenty groundmass samples were obtained from basalts and basaltic andesites collected from lavas as showed in Fig. 2 and Table 1.

These samples were dated by using the step-heating $^{40}Ar/^{39}Ar$ method. In order to constrain the eruption age and avoiding excess argon, a binocular microscope was used to carefully remove the 60–80 mesh granules of processed groundmass. $^{40}Ar/^{39}Ar$ measurements were performed at Institute of Geology and Geophysics of Chinese Science Academy (IGGCAS), Beijing. A number of neutron fluence monitors (standards) have been intercalibrated at $^{40}Ar/^{39}Ar$ Lab. of IGGCAS [38]: relative to 18.6 Ma Brione muscovite monitor [39], nine total fusion analyses of Mt Dromedary (NW Wales, Australia) biotite (Ga 1550), gave a mean age of 98.5±0.6 Ma, consistent with the 98.5±0.8 Ma and 98.8±0.5 Ma ages determined by Spell and McDougall [40] and Renne et al. [41] respectively.

Groundmass wafers weighing between 3–16 mg, multiple samples of the 18.6±0.4 Ma neutron fluence monitor mineral Brione muscovite were irradiated *in vacuo* within a cadmium-coated quartz vial for 45.8 h in position H8 of the facility of Beijing Atomic Energy Research Institute reactor (49-2). Six to eight replicate analyses of the monitors from each position in the vials were conducted to constrain the vertical neutron fluence gradient to within ±0.7%. This additional uncertainty was propagated into the plateau and inverse isochron ages. However, complete external errors including those arising from the decay constants and primary K–Ar standards were not propagated.

Interfering nucleogenic reactions were checked for every irradiation by using CaF and K_2SO_4,. The correction factors in this study are $[^{36}Ar/^{37}Ar]Ca=0.000261\pm0.000014$; $[^{39}Ar/^{37}Ar]Ca=0.000724\pm0.000028$; $[^{40}Ar/^{39}Ar]K=0.000880\pm0.000023$. Mass discrimination was monitored using an on-line air pipette from which multiple measurements are made before and after each incremental-heating experiments. The mean over this period is 1.00831±0.00017 per amu and the uncertainty of this value is propagated into all age calculations.

Groundmass wafers were placed into a Ta tube resting in the Ta crucible of an automated double-

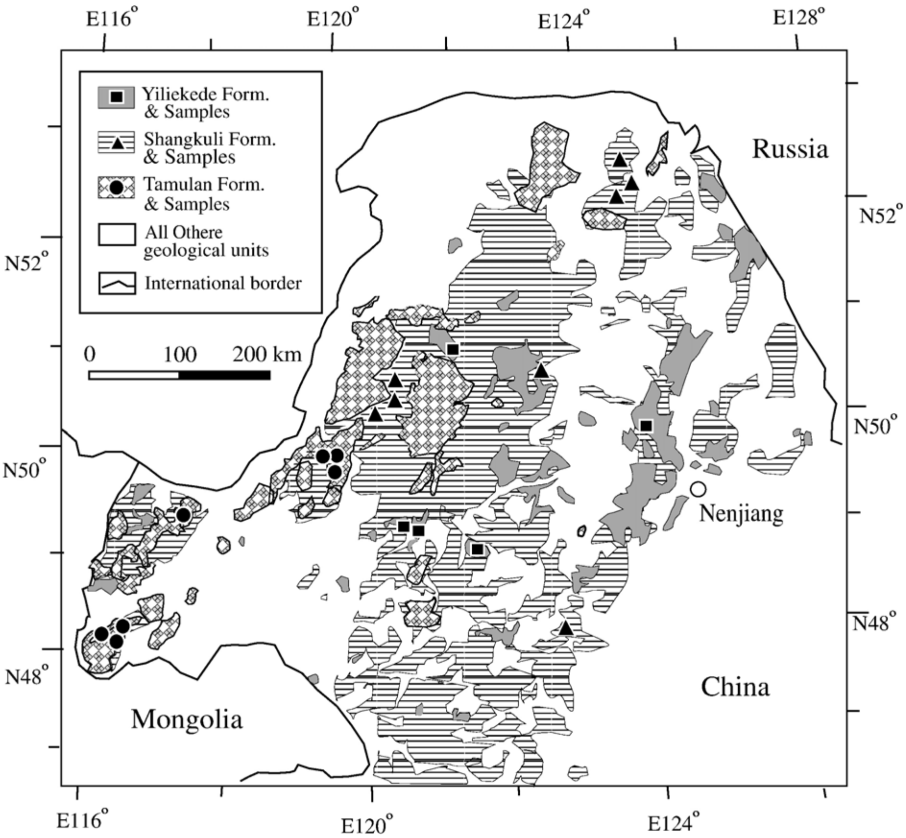

Fig. 2. Detailed volcanic distribution in NEC and sampling spots.

Table 1
$^{40}Ar/^{39}Ar$ dating results

Sample	Rock	Formatio	Position	Plateau age(Ma)	Inverse isochron age(Ma)	Integrated age(Ma)	$^{40}Ar/^{39}Ar$ Initials
MZL04-6	Basalt	Tamulan	49°28′22″E 117°25′42″N	160.0±0.8	160.0±0.9	161.0±0.8	298±6
MZL10	Basalt	Tamulan	48°16′09.9″E 116°15′17.2″N	162.6±0.7	162.4±0.8	160.7±0.7	299±19
MZL13	Basaltic andesite	Tamulan	48°15′37.1″E 116°16′32.2″N	162.0±0.8	162.1±1.2	162.0±0.8	337±46
MZL16	Basalt	Tamulan	48°14′01.2″E 116°17′48.2″N	147.0±0.8	146.5±0.8	151.3±0.8	266±32
ERBY04-1	Basalt	Tamulan	49°50′32″E 119°57′34″N	139.7±0.7	140.7±1.1	139.7±0.7	273±16
ERBY04-4	Basaltic andesite	Tamulan	49°50′47″ E 119°57′37″N	140.3±0.7	142.4±1.0	139.5±0.7	270±19
ERBY1-9	Basalt	Tamulan	49°50′32″E 119°57′35″N	142.7±0.7	142.9±0.7	142.1±0.7	286±27
GH07	Basalt	Shangkuli	50°19′54″E 120°14′52.7″N	123.3±0.6	123.4±0.9	124.9±0.6	305±9
GH10	Basalt	Shangkuli	50°26′22.6″E 120°48′12.6″N	121.2±0.6	120.9±0.7	122.1±0.6	340±71
TH08	Basalt	Shangkuli	52°19′30.2″E 124°40′39.7″N	123.7±0.6	124.5±0.8	122.8±0.6	270±24
TH24	Basaltic andesite	Shangkuli	52°39′37.7″E 124°19′38.1″N	125.6±0.6	123.7±1.6	125.8±0.6	389±70
TH22	Basalt	Shangkuli	52°28′01″E 124°33′24.8″N	122.3±0.6	122.4±0.8	122.4±0.6	295±27
ELC04-1	Basalt	Shangkuli	50°40′04″E 122°35′57″N	124.5±0.6	124.7±0.7	126.0±0.6	292±8
ZLT04-8	Basalt	Shangkuli	48°00′10″E 122°46′20″N	122.2±0.6	121.7±0.7	122.4±06	302±5
GH04-1	Basalt	Shangkuli	50°21′32″E 120°26′49″N	123.9±0.6	120.7±1.3	121.9±0.6	325±16
YKSNQ04-4	Basalt	Yiliekede	49°12′22″E 120°36′50″N	115.8±0.6	116.4±0.8	115.7±0.6	289±9
GH04-4	Basalt	Yiliekede	50°59′17″E 121°19′16″N	114.5±0.6	114.3±0.7	115.2±0.6	299±5
YKS04-3	Basalt	Yiliekede	48°50′40″E 121°34′50″N	106.2±0.6	106.1±1.1	101.2±0.5	294±7
JGD04-4	Basalt	Yiliekede	49°56′53″E 124°22′48″N	115.3±0.6	116.0±0.6	114.6±0.6	286±6
YKSNQ04-1	Basaltic andesite	Yiliekede	49°12′47″E 120°36′50″N	–	114.3±1.0	113.2±0.6	300±11

vacuum resistance furnace. These were incrementally-heated in 15 steps of 10 min each from 700 or 750 °C to 1400 or 1500 °C. Following 5 additional minutes of gas purification on Al–Zr getters, isotopic measurements were made on a mass spectrometer MM5400 with a Faraday cup and an electron multiplier of which the latter was used as the collector during this study. Hot system blanks determined several times each day prior to degassing the samples were typically 3×10^{-16} mols of ^{40}Ar and 9×10^{-19} mols of ^{36}Ar in nearly atmospheric ratios and 2–3 orders of magnitude smaller than sample signals [42]. Although the mean blank errors were generally ~2% for ^{40}Ar and ~5% for ^{36}Ar, the large size of the samples relative to the blank minimized the impact of propagating these errors into the final age calculations.

Plateau ages were determined from 3 or more contiguous steps, comprising >50% of the ^{39}Ar released, revealing concordant ages at the 95% confidence level. The uncertainties in plateau ages reflect multiplication by the MSWD and were obtained by standard weighting of errors for individual steps according the variance [43]. Thus, more precise determinations were given greater weight than those of lower precision and the overall uncertainty about the mean value may be greatly reduced. Because no assumption is made

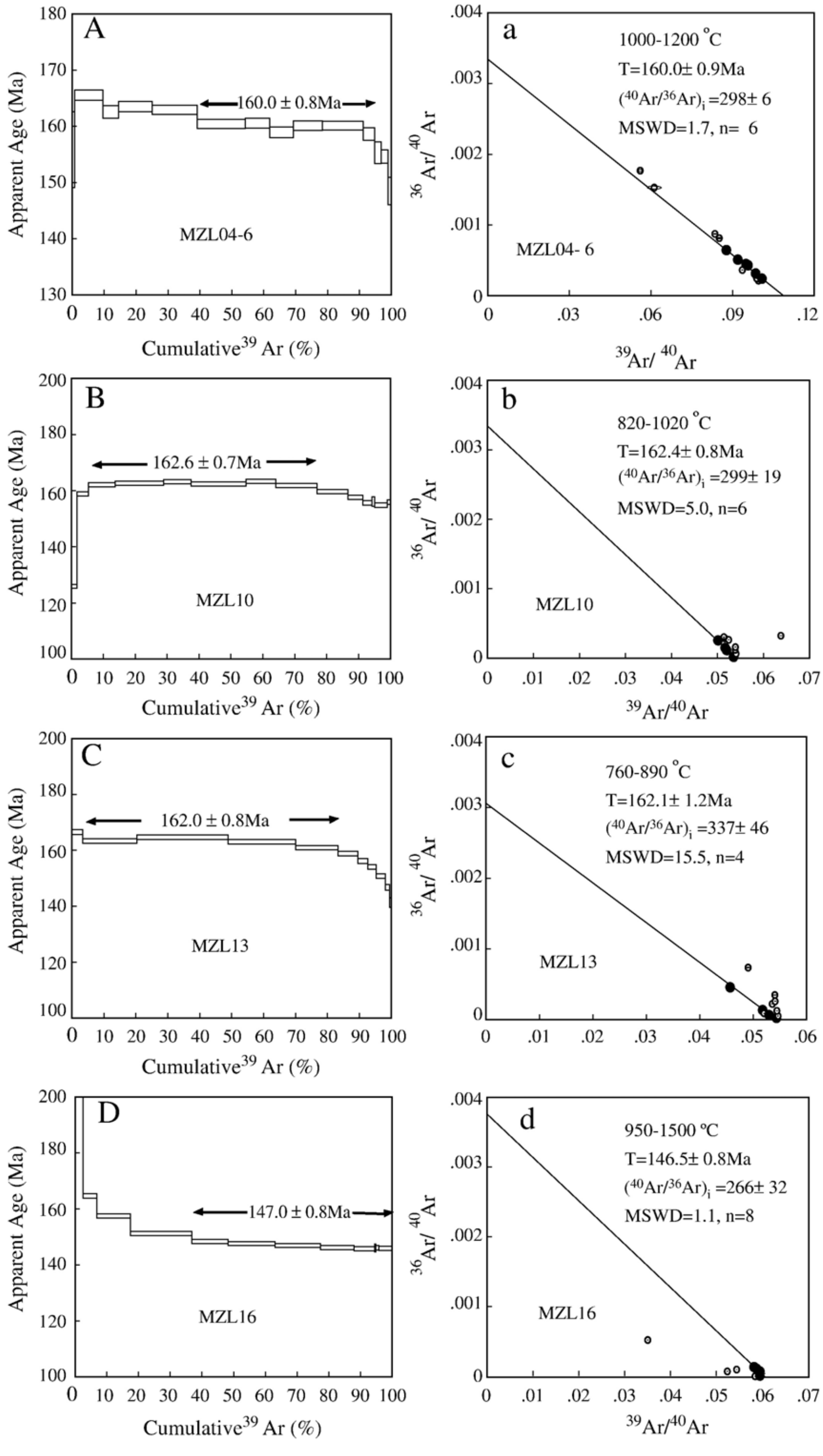

Fig. 3. Age spectra (A–G), and isotope correlation (a–g) diagrams of samples from Tamulan formation. The plateau ages are indicated by the arrows. The solid circle denote the steps used in fitting inverse isochron. 2 sigma errors are quoted for the points plotted in isotope correlation diagrams.

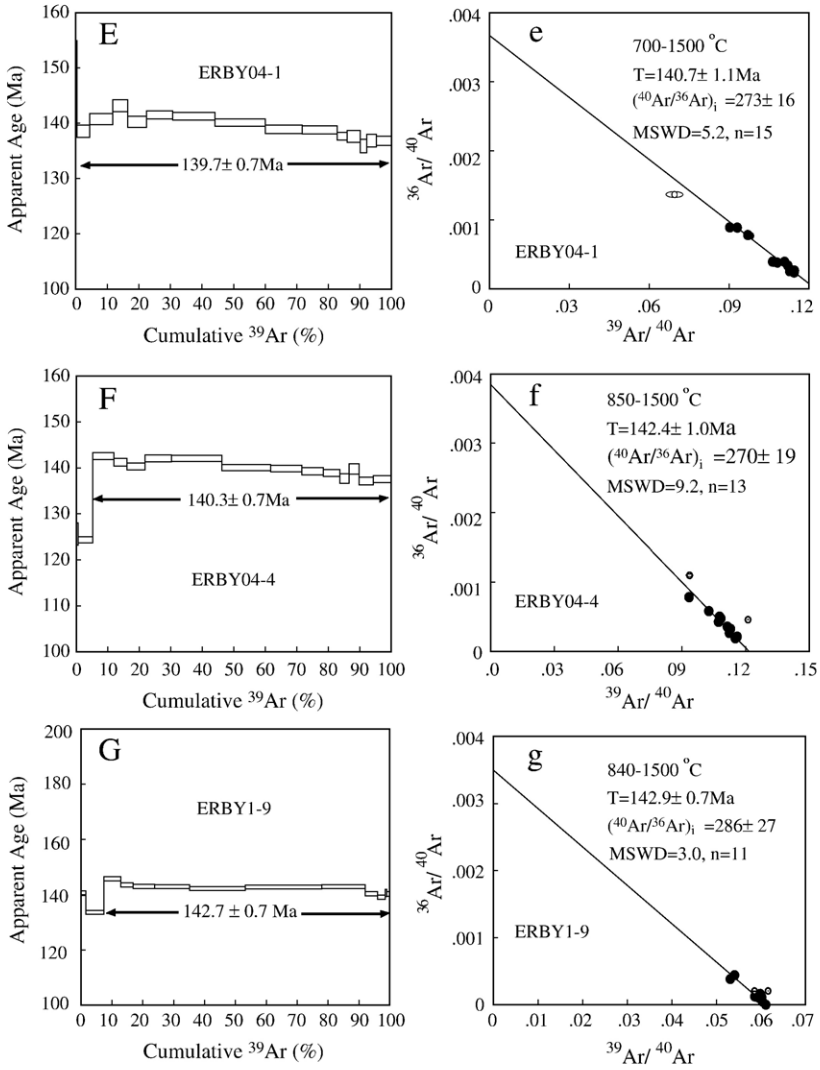

Fig. 3 (*continued*).

regarding the trapped component, the preferred ages are inverse isochrones, calculated from the plateau steps using the York [44] regression algorithm. Errors are reported at the 2σ confidence level. Analyses results are provided in the Supplementary data table.

4. $^{40}Ar/^{39}Ar$ analysis results

The age results from the step-heating experiments are presented in Table 1. The age spectra and isotope correlation (inverse isochron) diagrams are illustrated in Figs. 3–5. For each sample the argon release age spectra and inverse isochrones are presented. Both the plateau and inverse isochron age uncertainties are given at 2σ level, and do not include systematic errors related to standards or the ^{40}K decay constants, which should be considered if these results are compared to ages estimates obtained from other radioisotopic systems [45].

In the following section, we will first have a general evaluation of data quality, and then discuss the ages of every formation separately.

4.1. The $^{40}Ar/^{39}Ar$ data

Most of the samples present well-resolved plateaus, consistent inverse isochron ages and initial $^{40}Ar/^{36}Ar$ ratios indistinguishable from the atmospheric value (295.5) (Table 1, Figs. 3–5). However, some of the age spectra are complicated and may warrant further discussions. ^{39}Ar loss in the $^{40}Ar/^{39}Ar$ dating of groundmass of volcanic rocks is a common phenomenon and can be seen in this study. Samples yielding

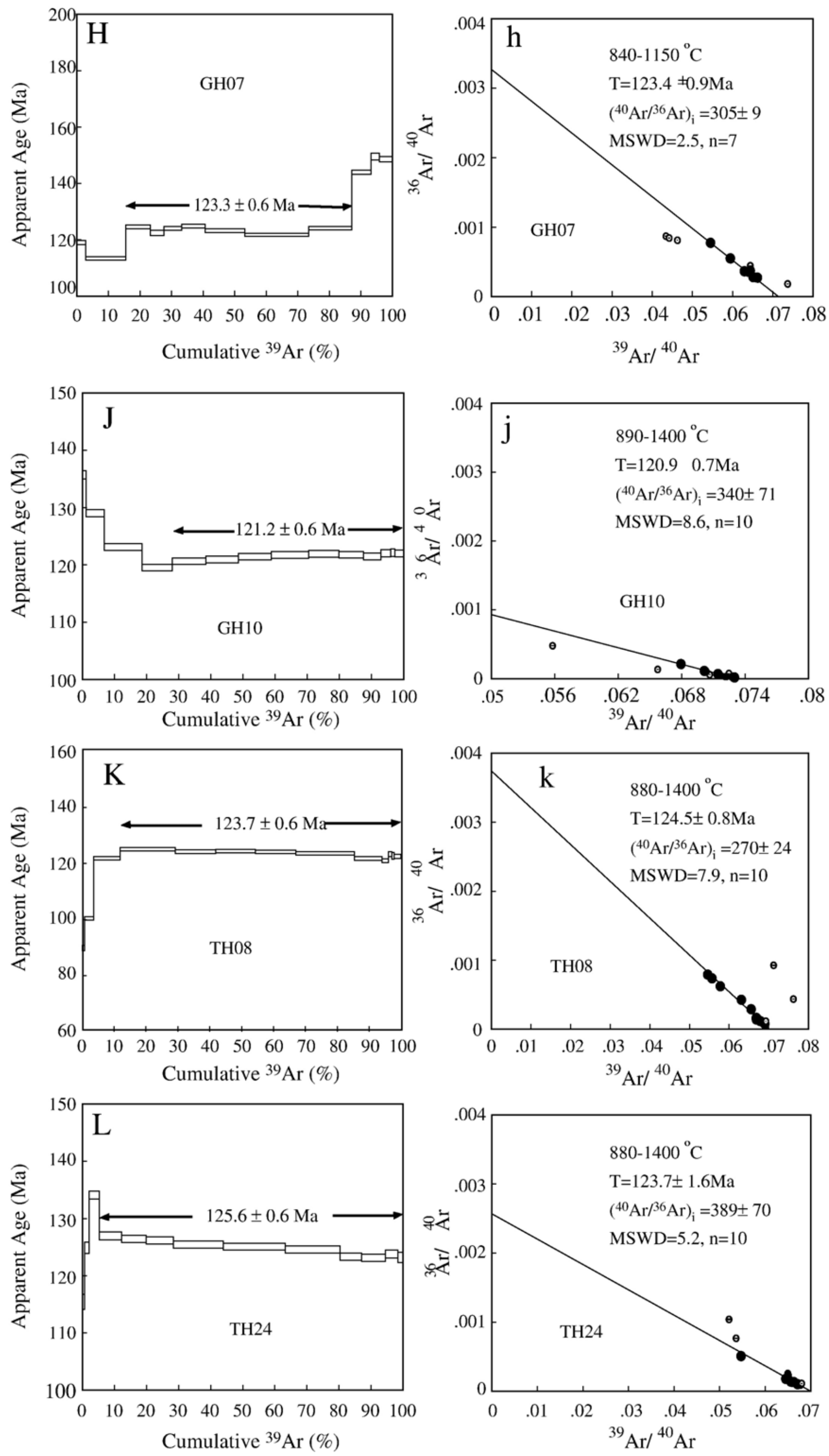

Fig. 4. Age spectra (H–P), and isotope correlation (h–p) diagrams of samples from Shangkuli formation. The plateau ages are indicated by the arrows. The solid circle denotes the steps used in fitting inverse isochron. 2 sigma errors are quoted for the points plotted in isotope correlation diagrams.

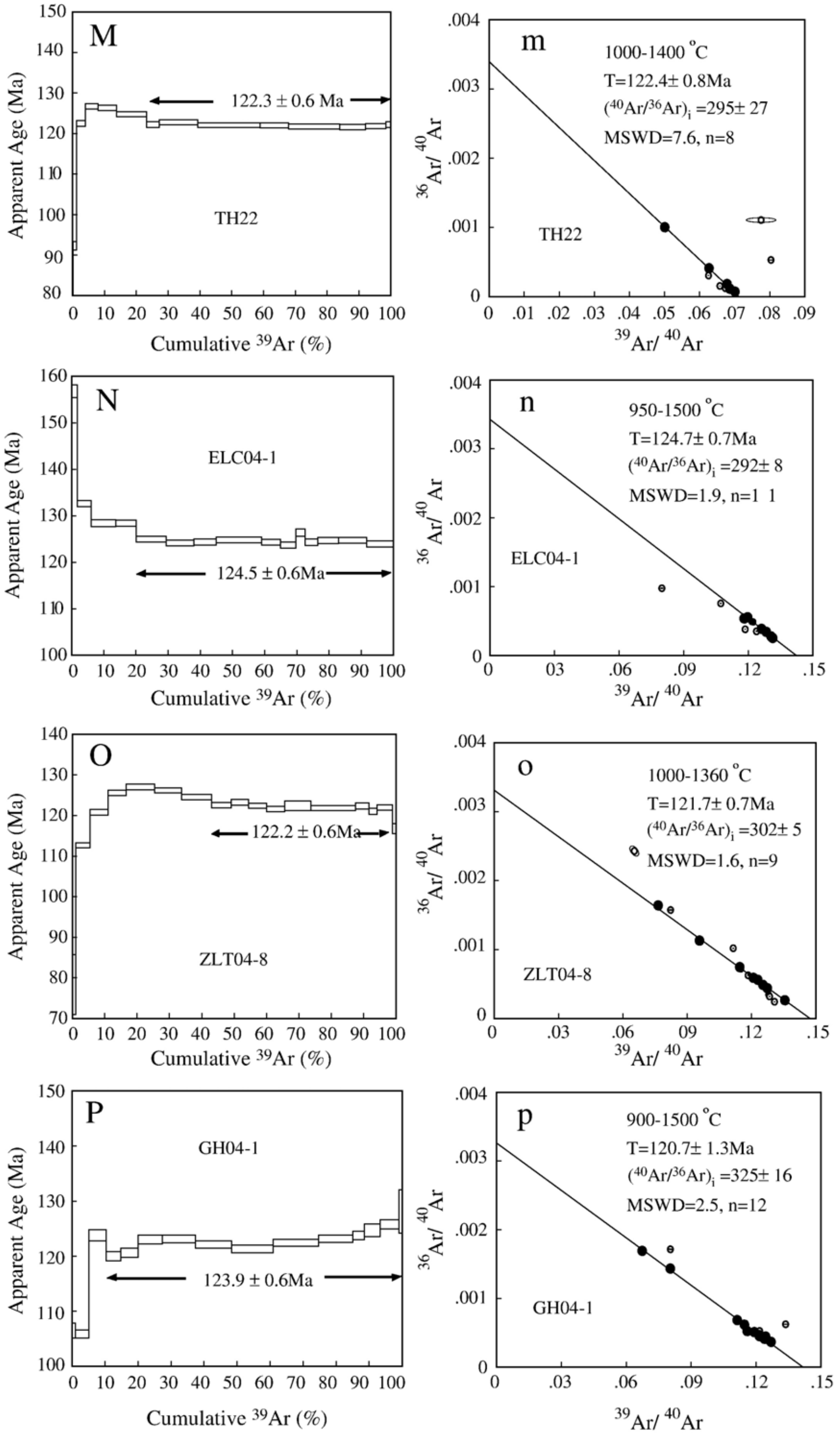

Fig. 4 (*continued*).

characteristics age spectra that typically display high apparent ages for the low-temperature steps, or low apparent ages for the high temperature steps have found and discussed in some groundmass $^{40}Ar/^{39}Ar$ dating works [46–48]. The low temperature discordant sections start at high apparent ages that monotonically decrease towards the age plateau (e.g. MZL16 in Fig. 3 and ELC04-1 in Fig. 4); or the high temperature ages decrease from the age plateau to the abnormal low values (such as MZL13 and MZL04-6 in Fig. 3). This observations can be explained by the recoil of $^{39}Ar_k$ (increasing the apparent ages) in combination with the preferential degassing of alteration phases (increasing the atmospheric component) that are located interstitially and in the surface of plagioclase or clinopyroxene in the groundmass [47]. The intermediate temperature

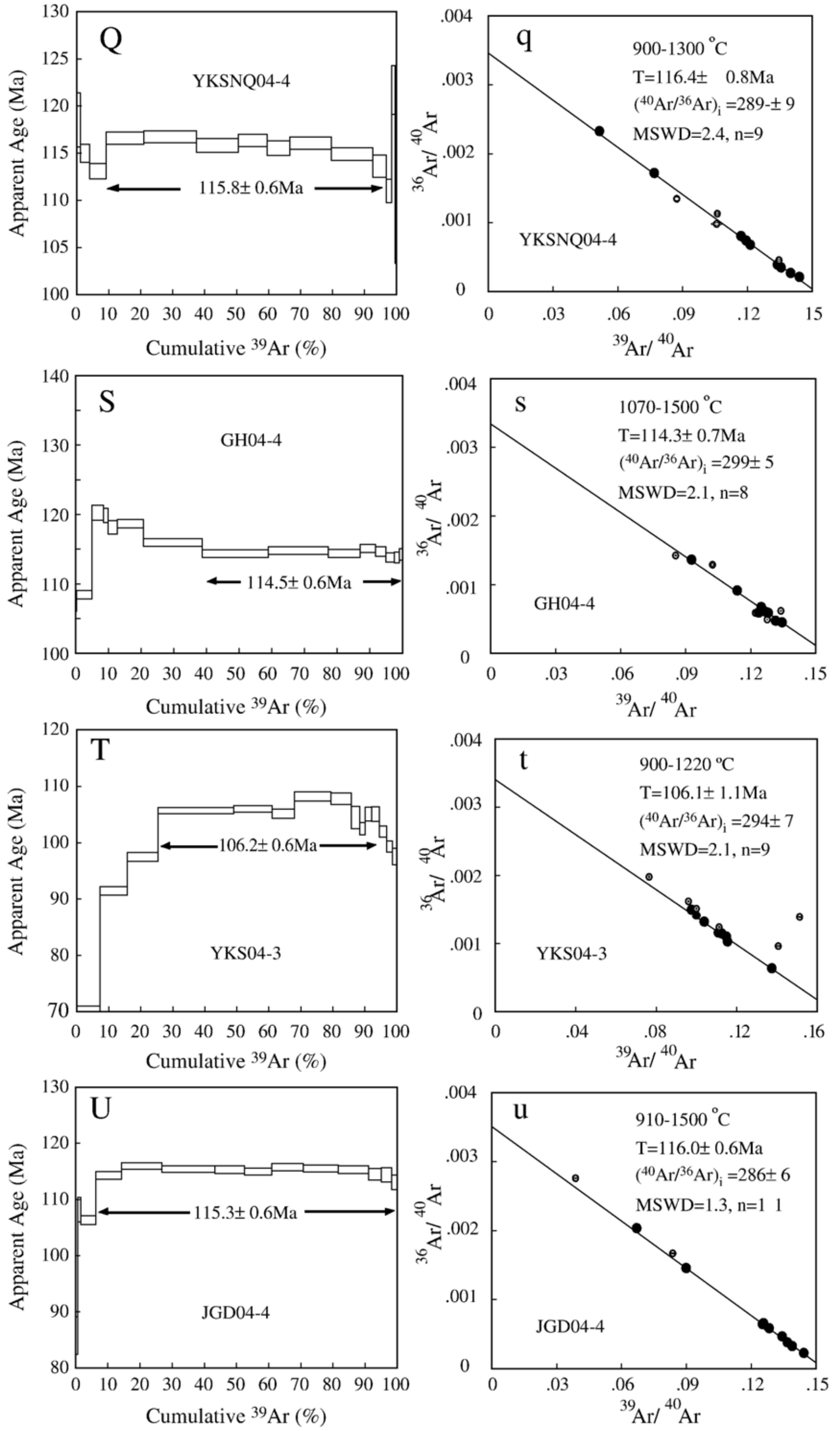

Fig. 5. Age spectra (Q–V), and isotope correlation (q–v) diagrams of samples from Yiliekede formation. The plateau ages are indicated by the arrows. The solid circle denotes the steps used in fitting inverse isochron. 2 sigma errors are quoted for the points plotted in isotope correlation diagrams.

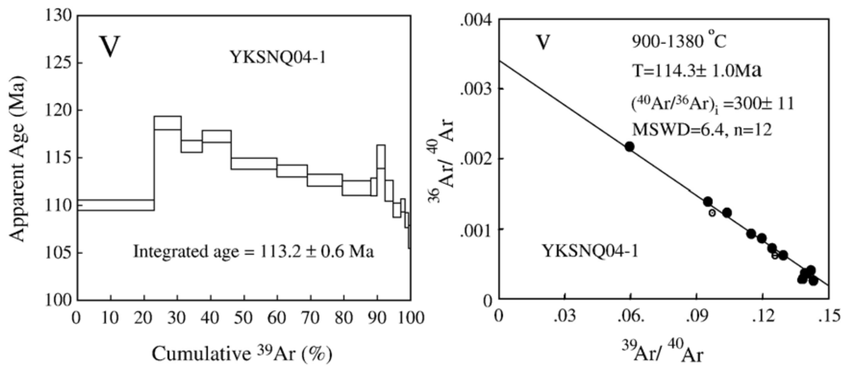

Fig. 5 (*continued*).

steps exhibit age plateaus that are high in their radiogenic component (90–100%). This may suggest the effects of alteration and $^{39}Ar_k$ recoil to the plateau portions of the age spectra are negligible [48]. This is confirmed by the fact in this study that all plateau ages are consistent with their inverse isochron ages at the 2σ confidence level and that $^{40}Ar/^{36}Ar$ intercept values are indistinguishable from or slightly lower than the 295.5 atmospheric ratio (Table 1), ruling out excess ^{40}Ar.

It seems that the argon release pattern of YKSNQ04-1 cannot be explained by ^{39}Ar loss from the recoil simply, because the lowest temperature step accounting for more than 20% of released argon, shows lower age (110.0 Ma, supplement table, Fig. 5V) than most higher temperature steps. This pattern may be a result from combination effect of ^{39}Ar recoil and ^{40}Ar loss from alteration. Although no meaningful plateau can be obtained, the intermediate temperature steps show a well-defined inverse isochron (Fig. 5v) with intercept age of 114.3 ± 1.0 Ma, consistent with the integrated age (113.2 ± 0.6 Ma, Table 1 and Fig. 5V).

On the contrary, alteration of the minerals may cause the strong loss of ^{40}Ar from the crystals, and we will observe argon release patterns characterized by low apparent age for the low-temperature steps, such as sample YKS04-3 (Fig. 5T). The 30% of the released argon was affected apparently by such loss (Fig. 5T) and it cannot immediately eliminate such affect at the higher temperature steps, therefore, the plateau at the higher temperature steps of YKS04-3 should be the minimum limit of the "real age" which may be the reason showing ~ 10 Ma lower in age than those from same formation (Yiliekede).

The age spectrum of sample GH07 seems exhibiting ^{40}Ar loss pattern at first glance which shows the highest ages at the highest temperature steps (Fig. 4H). But only two steps (~ 18% of released argon) show lower ages, and importantly the first (lowest temperature) step shows higher age (~ 120 Ma) than the second (higher temperature) step (~ 115 Ma) suggesting that the ^{40}Ar loss may not be the reason for these two lower ages. This is confirmed by the wide plateau (> 70% of argon released) for the following higher temperature steps. Therefore, the highest three apparent ages at highest temperature steps, we prefer to explain these highest apparent ages by excess argon trapped in anion sites [49]. It was reason that at high temperatures of laboratory extraction the excess argon would be trapped in anion sites of the mineral structure [49]. Supporting evidences for this mechanism was offered by Claesson and Roddick [50], who showed that the release of excess argon ^{40}Ar from calcic plagioclases at high temperature was accompanied by chlorine-derived ^{38}Ar suggesting that they originated from anion sites.

4.2. Dating results

4.2.1. Tamulan formation

Seven samples (MZL04-6, MZL10, MZL13, MZL16, ERBY 04-1, ERBY04-4 and ERBY1-9) were collected from the Tamulan Formation (Fig. 2), which yielded well-defined age spectra with plateau ages in two ranges from 160.0 ± 0.8 to 162.6 ± 0.7 Ma and 139.7 ± 0.7 to 147.0 ± 0.8 Ma (Table 1, Fig. 3). Apart from ERBY04-4, all these plateau ages are quite consistent with their respective intercept ages (Table 1, Fig. 3) obtained from the isotope correlation diagrams (Fig. 3). Regression of the data on the isotope correlation diagram indicate that the trapped initial $^{40}Ar/^{36}Ar$ ratios are, as shown in Table 1 and Fig. 3, suggest no measurable excess argon was caught when they erupted. Fig. 3f shows that the inverse isochron age for ERBY04-4 is 142.4 ± 1.0 Ma, which is a little higher than its plateau age 140.3 ± 0.7 Ma (Fig. 3F). The initial $^{40}Ar/^{36}Ar$ ratio of this sample, 270 ± 19, is apparently lower than the atmospheric value, implying that the background contribution in the data and should be considered when interpreting plateau age. As no assumptions are made about the initial $^{40}Ar/^{36}Ar$ ratios on the inverse isochron age, we regard that the inverse isochron age of ERBY04-4, 142.4±1.0 Ma, is preferred.

The dating result of samples from Tamulan formation clearly show that they are in two distinct duration: from ~160 to ~163 Ma and ~140 to ~147 Ma. This suggests that the lavas which were previously defined as "Tamulan Formation" [12] may not be the real one formation. But in this paper, we follow the tradition to use the term "Tamulan Formation" for these lavas of two periods.

4.2.2. Shangkuli formation

Eight samples (GH07, GH10, TH08, TH24, TH22, ELC04-1, ZLT04-8 and GH04-1) were collected from Shangkuli formation at different sites (Fig. 2). Six samples show fine-defined age spectra over 70% of ^{39}Ar released (Fig. 4) giving a plateau age range from 121.2±0.6 to 124.5±0.6 Ma (Table 1, Fig. 4). Apart from TH24 and GH04-1, the samples exhibit consistent inverse isochron ages (Table 1, Fig. 4) with their plateau ages respectively. The initial values of $^{40}Ar/^{36}Ar$ of these samples agree with that of the air (Table 1, Fig. 4) suggesting they trapped only atmospheric argon when they formed. TH24 and GH04-1 show different spectrum ages with inverse isochron ages as well as initial $^{40}Ar/^{36}Ar$ values higher than atmospheric value (389±70 and 325±16 respectively, Table 1 and Fig. 4). This implies that excess argon was trapped when they formed. Therefore, we regard the inverse isochron age as being more objective, as no assumptions are made about the initial $^{40}Ar/^{36}Ar$ ratios.

These dates suggest that the Shangkuli formation was formed during ~120–~125 Ma.

4.2.3. Yiliekede formation

Five basaltic rocks (YKSNQ 04-4, GH04-4, YKS04-3, JGD04-4 and YKSNQ04-1) were sampled from Yiliekede formation in different localities (Fig. 2). Four of these samples (YKSNQ 04-4, JGD04-4, and GH04-4) yielded age spectra with plateau ages from 106.2±0.6 to 115.8±0.6 Ma (Table 1, Fig. 5). In the $^{36}Ar/^{40}Ar$ versus $^{39}Ar/^{40}Ar$ correlation diagrams (Fig. 5), the data of the four samples define intercept ages consistent with their respective plateau ages (Table 1); and the $^{40}Ar/^{36}Ar$ initial ratios are quite consistent with the atmospheric $^{40}Ar/^{36}Ar$ ratio (295.5) as well (Table 1, Fig. 5). However, dating on the sample YKSNQ04-1 shows no statistically meaningful plateau age (Fig. 5V), but its consistent integrated age (113.2±0.6 Ma) and inverse isochron age (114.3±1.0 Ma), and initial $^{40}Ar/^{36}Ar$ (300±11) indistinguishable from atmospheric value suggest these ages are reasonable.

The sample YKS04-3 show a much lower age than those from the same formation. As discussed above, this may be caused by the ^{40}Ar loss from the alteration. Therefore, if exclude YKS04-3, the dating results from

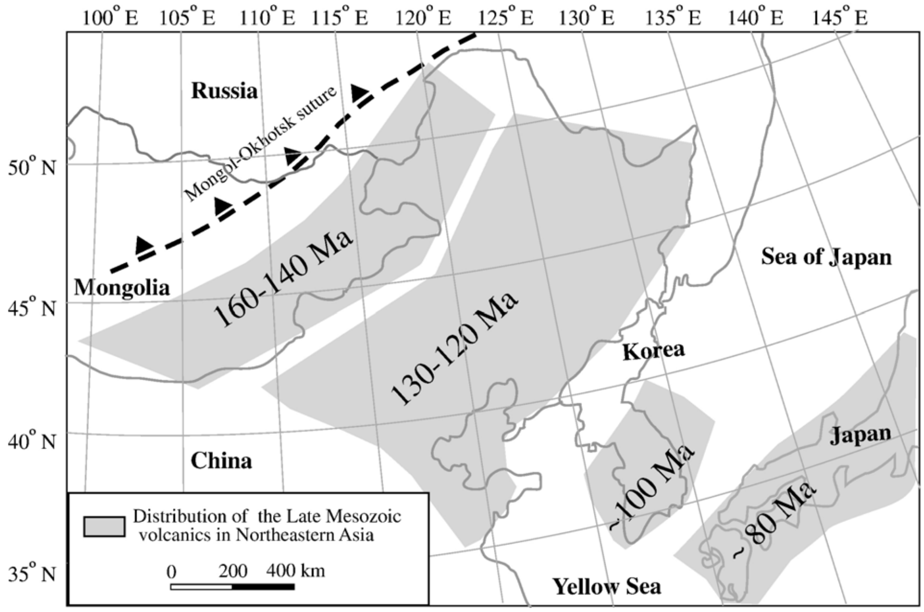

Fig. 6. The sketch shows the spatial and temporal trends of peak magmatism in NE Asia, strongly suggesting an eastwards migration from southeastern Mongolia—Great Xin'an Range to the southwestern Japan. Data come from the age compilations and summaries in [2,6,10,11] and this study.

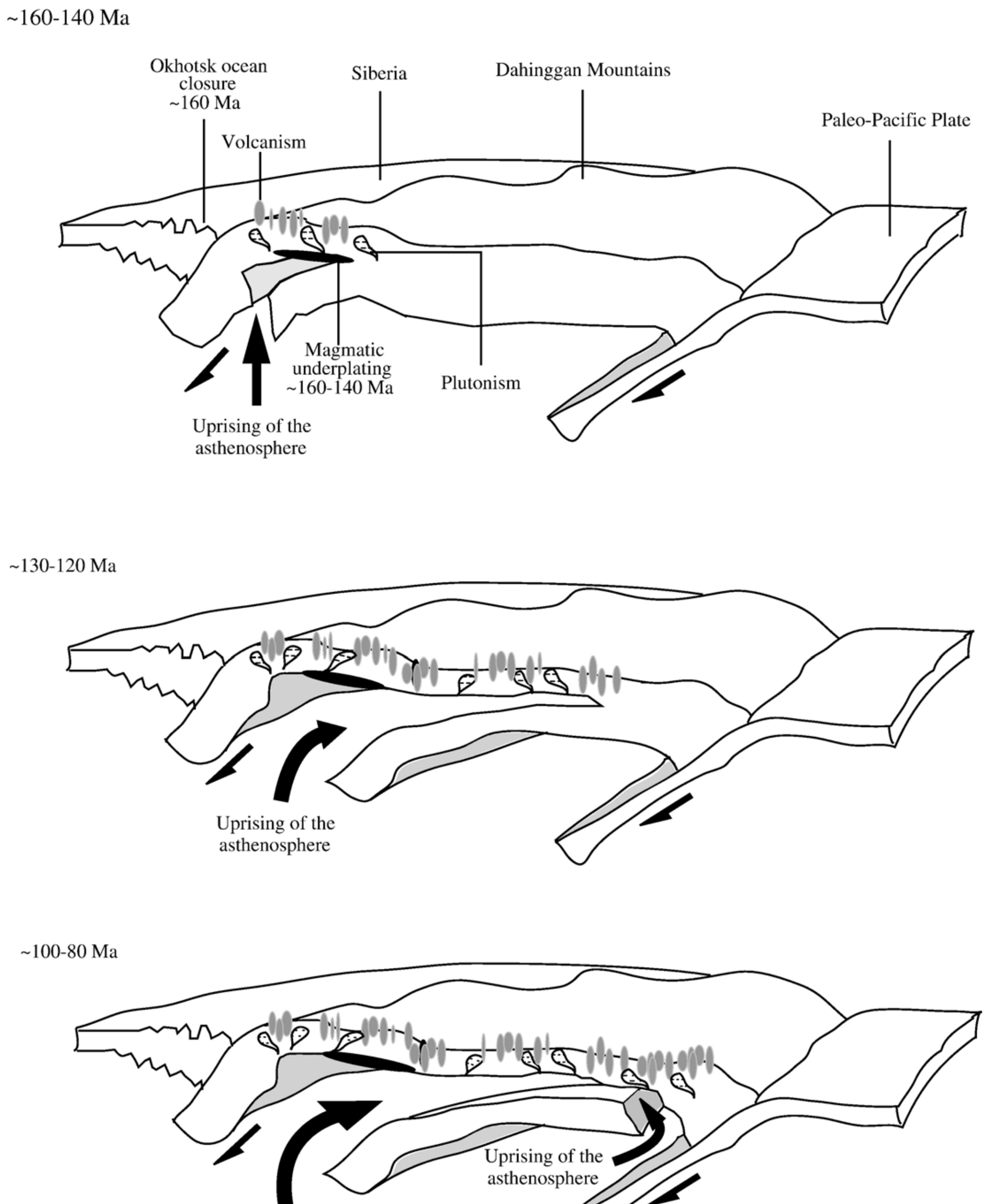

Fig. 7. Speculative geodynamic scenario of northeastern Asia during Late Mesozoic. ~160–140 Ma: the closure of Mongol–Okhotsk Ocean obstracted the movement of the northeast China–Mongolia block from the subduction of paleo-Pacific plate; the thickened lithosphere started to delaminate from the west edge of the block due to the strong strain, this resulted in the upwelling of the asthenosphere and induced magmatism and undrplating. ~130–120 Ma: as the delamination propagated eastwards like an opening shears, the magmatism propagated eastwards. ~100–80 Ma: continued propagation of delamination and magmatism. This course ended until the delaminated lithosphere detached completely. See text for details.

Yiliekede formation indicate that the eruption of the formation was constrained in a duration between ~113 and 116 Ma.

5. Discussion

5.1. The volcanic succession in the Great Xing'an Range

Geologists believed that there was evidence of continuous volcanic eruption in the Tamulan Formation during the Late Jurassic time (~160) and throughout the Late Jurassic–Early Cretaceous times (~160–~90) in the Great Xing'an Range. This belief was based on data from widespread volcanic bodies of ages determined by Rb–Sr and Sm–Nd dating methods [7,12,51]. A recent study [6] showed that this giant igneous event in the Great Xing'an Range can be constrained in a short duration of 10 Ma from ~120 to ~130 Ma, based on U–Pb dating on intrusive bodies. However, the results of our dating on the three main volcanic formations in the Great Xing'an Range do not supported these views.

Our dating indicates that the three main formations, Tamulan, Shangkuli and Yiliekede, formed in short durations of ~163–160 and ~147–140, ~125–120, ~116–113 Ma respectively. But it should be noted that this conclusion need to be ascertained by the further work due to the representation of the samples. Tanmulan Formation indicates the start of the igneous activity during the Late Jurassic time in this region.

5.2. Migration of Late Mesozoic volcanic activity in Northeast Asia

Volcanism during the Late Mesozoic time occurred not only in the Great Xing'an Range, but widespread in NEC and its adjacent areas, such as south and east Mongolia, the Korean Peninsula and southwest Japan. Our dating results place a precise constraint on the timing of this volcanic succession and the main stage as the Great Xing'an Range for the first time. These data, combined with recent age compilations of igneous activity in the adjacent regions [2,6,10,11], strongly suggests that igneous activity migrated from west to east in Northeast Asia during the Late Mesozoic (Fig. 6). This migration was constrained between the Mongol–Okhotsk suture and Pacific Plate subduction zones.

In south and east Mongolia, southeast of the Mongol–Okhotsk suture, the volcanic activity continued for the past 160 Ma peaking around 160–140 Ma [10]. Largely based on the K–Ar 10 isotopic ages of the volcanic successions, there is marked similarity in compositional parameters of most of the volcanic rocks throughout the entire period of formation of this region. The various volcanic associations are dominated by basic rocks, accounting for no less than 95% of the total volume of the volcanic rocks [10]. They are presented by subalkaline olivine-basalts and alkali basaltoids, displaying geochemistry similar to that of their equivalents in northern China. Study of isotopic composition of these volcanic rocks and associated mantle xenoliths like iherzolites suggests that their primary melts were derived from the lithospheric mantle [10].

Volcanic rock also spread in Yanshan range, south of the Great Xing'an Range (Fig. 1), with a cumulative thickness of the volcanic succession up to ~4 km [14]. Zircon U–Pb ages and $^{40}Ar/^{39}Ar$ plateau ages for the volcanic rocks [52–59] constraint a duration of 130–150 Ma, with a peak of ~135–145 Ma. They take similarities with those in the Great Xing'an Range geochemically and petrologically.

To the east of the Great Xing'an Range lies the Songliao basin, the largest oil- and gas-producing basin in China. Mesozoic igneous rocks are widespread throughout the basin. The newly obtained core section from drilling and high-quality deep seismic reflections in recent years provide good selection of samples and better understanding of the structure of the volcanic successions buried in the basin. Recent $^{40}Ar/^{39}Ar$ and K–Ar ages [11] revealed that the volcanic activities mainly were during 120–130 Ma.

Late Mesozoic volcanic rocks are also widespread in the Liaoxi area (Western Liaoning Province) to the south of Songliao Basin. Recently obtained ages for the volcanics from this area concentrate mostly between 128.4 ± 0.2 to 120.3 ± 0.7 Ma [42,53,54,60–63]. The compilation of ages younger than 150 Ma, including those of intrusive rocks, indicates that 120–130 Ma is the peak time of igneous activity in this area [6].

Based on the description above, a general view of the spatial and temporal distribution for Late Mesozoic volcanic activity in the NEC and its adjacent area can be derived. From west to east, the peak time of igneous activities changed from 160–140 Ma (in east Gobi of Mongolia and west Great Xing'an Range) to 120–130 Ma (Songliao–Liaoxi area and Liaodong peninsula), suggesting supporting the migration of volcanic front in the Late Mesozoic time in NEC and its adjacent areas.

It is worthy to note that the migration of magmatism eastwards is a common feature along east Asian continental margin, including eastern coast of China, Korea peninsula and southwest Japan [2,4]. Igneous rocks intruded in the east of Jiaodong peninsula of China and

Gyeongsang Basin of Korea aged mainly ~100 Ma in late Early Cretaceous, and further eastwards to vast region of southwest Japan the magmatism mainly aged ~80 Ma [2]. This pattern of magmatism along the eastern Asia continental margin was attributed to the ridge subduction [2] or angle-changing [4] of paleo-Pacific plate. However, they cannot explain the above phenomena observed in the inland of NEC and its adjacent areas.

5.3. Mechanism for the Late Mesozoic magmatism in northeastern Asia

The data present above indicate that the igneous activity in northeastern Asia had migrated from west to east, i.e. from central and east Mongolia and the Great Xing'an Range of China (~140–160 Ma) to Songliao–Liaodong region (120–130 Ma) to Korea peninsular (100 Ma), and farther to Southwest Japan (80 Ma). So what cause this migration? Here we discussed the deep processes under the frame of plate tectonics to attempt to explain the mechanism of magmatism migration in northeastern Asia.

The tectonic setting of NEC in the Late Mesozoic is still in dispute. Some characteristics of the volcanic rocks show that they are similar to those of island of continental marginal arcs [64,65]; however, there are many aspects that do not share the common features with arc volcanics [66]. On the researches of the chemical analysis of the rocks, the volcanics of NEC and its adjacent area do not show obvious compositional polarity, and incompatible elements mass fraction are higher than those of the typical arc volcanic rocks [5,17,64,66]. Recent study show that these rocks exhibits geochemical and Si, Nd isotopic characteristics similar to those of Cenozoic volcanism in the Basin and Range Province, USA, and are attributed to intraplate volcanism [5]. Importantly, most of volcanic rocks in NEC, especially in central and south of Mongolia, are far away (>1000 km) from the Mesozoic subduction zone of Pacific side, even the Japan Sea did not opened yet at that time. Therefore, it is difficult to explain the tectonic environment by a direct relation to the pacific plate subduction.

The wide occurrence of A-type granites and alkaline rocks of Late Mesozoic age in NEC and its adjacent area also suggests that the NEC was not in an compressive regime during that time [6]. For instance, several Early Cretaceous A-type granitic plutons have been reported in the Great Xing'an Range, such as Linxi A-type granitic bodies (145–111 Ma, Zircon U–Pb [67]), the Woduhe and Baerzhe bodies (129–122 Ma, Rb–Sr WR, [68]); in Zhangguangcailing range, examples are Baiushileizi [69], Lazishan [70] and Loushan [70] bodies in age range of 123–127 Ma (zircon U–Pb). In the southeast of NEC, Wulingshan, Qiancengbei and Jiashan A-type granites were reported of an age range of 113–132 Ma (zircon U–Pb, [52]). A carbonatite in Shandong was reported with K–Ar age on phlogopite of 122.9–122.5±0.7 Ma [71]. Since A-type granites and alkaline rocks developed either in post-orogenic or anorogenic setting, we propose their occurrence supports our contention that the NEC and its adjacent areas were in an extensional regime in the Late Mesozoic time.

Other evidences for the extensional setting in NEC and its adjacent areas in Late Mesozoic time come from the intrusion of dyke swarms, exhumed metamorphic core, and formation of basins. Dyke swarms are products of typhonic magmatism which may provide important information of the deep. Several dyke swarms have been reported [72], including Gufeng lamprophyre swarm (146.6±2.9 Ma, K–Ar on biotite, [72]), Linxi diabasic dyke swarm (100.6±2.7 Ma, K–Ar on biotite, [51]) in the Great Xing'an Range, and north Beijing bimodal dyke swarms (114–124 Ma K–Ar on biotite, [17,51]). The above cited ages of dyke swarms indicates their emplacement in the Early Cretaceous, synchronous with the development of intrusions and extrusions.

Early Cretaceous metamorphic core complexes were reported in China–Mongolia border areas [73,74] and in northeast Mongolia–Russia border region [75,76]. Exhumation of this complexes implies a rapid extension setting [9]. The timing is constrained by $^{40}Ar/^{39}Ar$ dating of synkinematic biotite at 129–126 Ma for the Yagan–Onch Hayrhan core complex at China–Mongolia border [74]. The K–Ar ages on biotites for all the gneiss granitoids of the core complexes at northeast Mongolia–Russia border place them between 110 and 140 Ma [76–78]. Apatite fission track thermo-chronology study of the Baikal–Mongolia region reveals a rapid cooling process from 140 Ma to 120 Ma, indicating that extensional denudation reduced the temperature of the deep-seated core to 120 °C at 140 Ma, and to 70 °C at 120 Ma [75]. The Early Cretaceous Yunmengshan, Miyun, Hohhot and Chengde metamorphic complexes are reported developed along Yanshan Mountains [9,52].

The age of detachment faults that controlled the Yiwulvshan and Louzidian–Dachengzi metamorphic complexes in Liaoxi is 127–116 Ma and 133–118 Ma respectively [79,80]. In the Liaodong peninsular, the Wazidian, yinmawanshan, Miaoling and Gudaoling plutons were emplaced along the detachment fault of the Liaonan metamorphic complexes [6], south Liaoning province.

5.4. A shears-shaped delamination model

It has been recognized that NEC and its adjacent areas was characterized by lithospheric thinning during the Mesozoic [14,23,31,34,35,81] and Os isotopic constrains indicates that this thinning was accomplished by delamination [35,82], coincide with the extension setting spatially and temporally. Therefore, it is vital to understand the tectonic regime controlling delamination and its link to widespread Mesozoic magmatism in NEC and its adjacent areas.

Several models have been proposed to explain the extensional features, widespread magmatism and lithospheric thinning. For example, Pacific backarc extension model [83–85], the hotpot and plume model [86,87], subduction model of Pacific Plate beneath eastern China [4,69,85,88,89], intraplate rifting model [90], Triassic collision model between the Yangze and North China cratons [23,35], and lithospheric mantle delamination model [6].

Backarc extension [83–85] may be the most popular view due to some arc signatures of the widespread calc-alkaline volcanic and I-type granitic rocks [4]. But this mechanism fails to account for the fact that Late Mesozoic extension occurred over a vast area, as manifested above, more than 2000 km from the Pacific subduction zone. The hotpot and plume model [86,87] argued that a mantle avalanche, induced by the closure of Tethys [91] and breakup of Gondwana [92] of 180 Ma ago, caused temperature rising in the upper mantle and ensuing erosion of the overlying lithospheric mantle from the rising asthenosphere. This resulted in lithospheric thinning. However, basalts and gabbros of mantle-derived mafic rocks, the predicted products of mantle plume activity, are rarely documented in the NEC and its adjacent areas [6]. A super plume was inferred around ~125 Ma [93], which may affected the whole earth. It has been proposed that the Early Cretaceous mid-Pacific super-plume increased subduction rates at its outer margins, which assisted in the lithospheric delamination in the eastern China [6], but it is hard to explain the magmatism migration.

Delamination of the lithospheric mantle will bring hot asthenosphere into contact with the Moho [94]. This should promote massive crustal melting and predicts a progressive migration of the resultant volcanism in the direction of delamination propagation [95]. The distribution of the massive igneous rocks in NEC and its adjacent areas temporally and spatially implies a possible relationship of the magmatism with the Pacific Plate subduction and the closure of Mongol–Okhotsk Ocean in some way. Therefore, we proposed a shears-shaped delamination model of the lithospheric mantle beneath NE Asia, induced by paleo-Pacific Plate subduction showing in Fig. 7. Continued subduction of paleo-Pacific Plate moved the Northeast China–Mongolia Block northwestwards, and the closure of Mongol–Okhotsk Ocean eventually led to collision between the Northeast China–Mongolia and Siberia by ~160 Ma [76]. This collision then obstructed the northwestward movement of the region, which shortened and thickened the lithosphere of NEC and its adjacent areas. The strain intensified gradually enough to have the thickened lithosphere delaminated at ~160 Ma starting from the southeast Mongolia—the great Xin'an Range, like a shears opened eastwards (Fig. 7). This led to asthenosphere upwelling, extensional tectonic setting, underplating, and ensued extensive magmatism activity propagation eastwards. The high degree of crustal melting accompanied the process to produce the geochemical and isotopic features discussed above. As the "shears" opened eastwards, alkali granitic plutonism became more pronounced, indicative of existence of voluminous magma ponds in the lower crust and involvement of mantle melts. The magmatic underplating played a crucial role in generation of the alkali granite plutons [96]. Climax of plutonism was then followed by widespread normal basins and formation of metamorphic core complexes in the upper crust. During ~130–120 Ma, the delamination reached its climax and left the most widespread volcanic formation (such as Shangkuli Formation in the Great Xing'an Range) in NEC.

Geochemical and timing evidences were reported for the magmatic underplating beneath the crust of northeastern China. Granulite xenoliths form the Cenozoic Hannuoba basalts, North China, was regarded as metamorphosed facies of magmatic underplating in northeastern China [97,98]. Zircons from these granulite xenoliths yielded two U–Pb age populations of ~160–140 and ~140–80 Ma [97,98]. Combination of Nd, Sr and Pb isotopic compositions, these two age periods were explained that the granulites were the products of ~160–140 Ma basaltic underplating and ~140–80 Ma granulite-facies metamorphism [98]. Those Precambrian protoliths underwent granulite-facies metamorphism at 150–80 Ma [98]. Zircons of magmatic origin from an olivine pyroxenite xenolith suggest basaltic underplating at 97–158 Ma [98]. The overlapping timing for the granulite-facies metamorphism and the basaltic underplating indicate that the Mesozoic granulite-facies metamorphism was induced by heating from the basaltic underplating at the base of the crust.

Recent studies on the tectonic transition from contractional to extensional deformation during Late

Mesozoic in NEC and its adjacent areas [9,99,100] lends further support to this interpretation. Studies on the basins and extensional structure in NEC and its adjacent areas show that contracted high-standing plateau caused by subduction of Pacific Plate and collision of north China and Siberia had transited from crustal compression to extension during 150–140 Ma [9,99,100]. This is consistent with the scenario of our shears-shaped delamination model.

6. Conclusions

Precise $^{40}Ar/^{39}Ar$ dating on volcanic succession of the Great Xing'an Range suggests that volcanism started ~160 Ma ago in the Late Mesozoic time, and indicates that the three main formations (Tamulan, Shangkuli and Yiliekede) formed in short durations of ~163–160, ~147–140, ~120–125, and ~113–116 Ma. Combined with the previous studies of data compilation on the widespread volcanic rocks in NEC and its adjacent areas, it reveals that the volcanism migrated from west to east in the whole northeast Asia, accompanied by the intrusions.

The close spatial-temporal relationship of these igneous rocks with metamorphic core complexes, intrusion of A-type granites and mafic dyke swarms, development of basins, suggests an extensional tectonic setting in NEC and its adjacent areas during Late Mesozoic.

An important magmatic underplating beneath NEC occurred during ~160–140 Ma, and the tectonic transition from crustal contraction to extension in North China timed around ~150–140 Ma, implies that the extension in NEC and its adjacent areas immediately followed the closure of the Mongol–Okhotsk Ocean.

A shears-shaped delamination mechanism for the geodynamic scenario beneath the northeast Asia is suggested, which states that the collision between north China–Mongolia and Siberia obstructed the westwards movement of the region from the subduction of paleo-Pacific plate, causing a rise of strain in the lithosphere and finally resulting in a shears-like lithospheric delamination starting from the west of NEC around at ~160 Ma ago. Then, mantle upwelling and underplating, leading to a crustal melting in an extensional setting, processed eastwards gradually in the whole Cretaceous, and induced the migration of volcanism.

Acknowledgment

We thank William Hanshumaker and Michalk Daniel for their assistance with the English grammar. We also thank reviewers for their thoughtful reviews. This work is supported by the Key Chinese National Natural Science Foundation (Grants No. 40334043) and Chinese National Natural Science Foundation (Grants No. 40473031).

Appendix A. Supplementary data

Supplementary data associated with this article can be found, in the online version, at doi:10.1016/j.epsl.2006.09.007.

References

[1] X. Zhou, R.L. Armstrong, Cenozoic volcanic rocks of eastern China-secular and geographic trends in chemistry and strontium isotope co position, Earth Planet. Sci. Lett. 59 (1982) 301–329.
[2] O. Kinoshita, Migration of igneous activities related to ridge subduction on Southwest Japan and the East Asian continental margin from the Mesozoic to the Paleogene, Tectonophysics 245 (1995) 25–35.
[3] O. Kinoshita, Possible manifestation of slab window magmatisms on Cretaceous southwest Japan, Tectonophysics 344 (2002) 1–13.
[4] X. Zhou, W. Li, Origin of Late Mesozoic igneous rocks in Southeastern China: implications for lithosphere subduction and underplating of mafic magmas, Tetonophysics 326 (2000) 269–287.
[5] W.X. Fan, F. Guo, Y. Wang, L. Ge, Late Mesozoic calc-alkaline volcanism of post-orogenic extension in the northern Dahinggan Mountains, northeastern China, J. Volcanol. Geotherm. Res. 121 (2003) 115–135.
[6] F. Wu, J. Lin, S.A. Wilde, X. Zhang, J. Yang, Nature and significance of the Early Cretaceous giant igneous event in eastern China, Earth Sci. Planet. Lett. 233 (2005) 103–119.
[7] Q. Lin, W. Ge, D. Sun, Tectonic significance of Mesozoic volcanic rocks in northeastern China, Sci. Geol. Sin. 33 (1998) 129–139 (in Chinese with English abstract).
[8] W. Ge, Q. Lin, D. Sun, Geochemical characteristics of the Mesozoic basalts in Dahinggan evidence of the mantle–crust interaction, Acta Petrol. Sin. 15 (1999) 396–407 (in Chinese with English abstract).
[9] Q. Meng, What drove Late Mesozoic extension of the northern China–Mongolia tract? Tectonophysics 369 (2003) 155–174.
[10] V.V. Yarmolyuk, V.I. Kovalenko, The Mesozoic–Cainozoic of Mongolia, in: A.B. Dergunov (Ed.), Tectonics, Magmatism, and Metallogeny of Mongolia, Taylor and Francis Group, London, 2001, pp. 203–244.
[11] P. Wang, W. Liu, S. Wang, W. Song, $^{40}Ar/^{39}Ar$ and K/Ar dating on the volcanic rocks in the Songliao basin, NE China: constraints on stratigraphy and basin dynamics, Int. J. Earth Sci. 91 (2002) 331–340.
[12] Bureau of Geology and Mineral Resources of Nei Mongolia Autonomous Region (BGMRNM), 1991. Regional Geology of Nei Mongolia Autonomous Region. Geological Publishing House, Beijing, 725 pp (in Chinese).
[13] J. Song, L. Dou, Mesozoic–Cenozoic Tectonics of Petroliferous Basins in Eastern China and Their Petroleum Systems, Petroleum Industry Press, Beijing, 1997, 182 pp.
[14] H. Xie, Tectonics of Accreted Terrane and Driving Mechanism, Science Press, Beijing, 2000, 256 pp.
[15] C.J. Hawkesworth, S. Turner, K. Gallagher, A. Hunter, T. Bradshaw, N. Rogers, Calc-alkaline magmatism, lithosphere

thinning and extension in the Basin and Range, J. Geophys. Res. 100 (1995) 10271–10286.

[16] N.W. Rogers, C.J. Hawkesworth, D.S. Ormerod, Late Cenozoic basalts magmatism in the Western Great Basin, California and Nevada, J. Geophys. Res. 100 (1995) 10287–10301.

[17] J. Shao, X. Li, L. Zhang, The geochemical condition for genetic mechanism of the Mesozoic bimodal dyke swarms in Nankou–Jiugongguan, Geochimica 30 (2001) 517–524 (in Chinese with English abstract).

[18] S.A. Graham, M.S. Hendrix, C.L. Johnson, D. Badamgarav, G. Badarch, J. Amory, M. Porte, R. Barsbold, L.E. Webb, B.R. Hacker, Sedimentary record and tectonic implications of Mesozoic rifting in southern Mongolia, Geol. Soc. Am. Bull. 113 (2001) 1560–1579.

[19] Y. Niu, Generation and evolution of basaltic magmas: some basic concepts and a new view on the origin of Mesozoic–Cenozoic basaltic volcanism in Eastern China, Geol. J. China Univ. 11 (2005) 9–46.

[20] D. Sun, X. Liu, C. Peng, Y. Liu, A Comprehensive Model for Kimberlite Prospecting in the North China Platform, Geological Publishing House, Beijing, 1993, 147 pp.

[21] J. Chi, F. Lu, L. Zhao, A Study of Primary Diamond Deposits in North China Craton: Genesis and Prospects, China Univ. Geosci. Press, Wuhan, 1992, 57pp.

[22] F. Lu, J. Zheng, W. Li, The mantle evolution pattern of Phanerozoic mantle in the eastern China: "The Mushroom Cloud" model, Geosci. Front. 7 (2000) 97–107.

[23] W.L. Griffin, A.D. Zhang, S.Y. O'Reilly, C.G. Ryan, Phanerozoic evolution of the lithosphere beneath the Sino–Korean craton, in: M.F.J. Flower, S.L. Chung, C.H. Lo, T.Y. Lee (Eds.), Mantle dynamics and plate interactions in East Asia, Am. Geophy. Union, Washington, D.C., Geodyn. Ser., vol. 100, 1998, pp. 107–126.

[24] Y. Song, F.A. Frey, Geochemistry of peridotite xenoliths in basalts from Hannuoba, eastern China: implications for subcontinental mantle heterogeneity, Geochim. Cosmochim. Acta 53 (1989) 97–113.

[25] Y. Song, F.A. Frey, Isotopic characteristics of Hannuoba basalt, eastern China: implication for their petrogenesis and the composition of subcontinental mantle, Chem. Geol. 85 (1990) 35–52.

[26] X. Zhi, Y. Song, F.A. Frey, Geochemistry of Hannuoba basalts, eastern China: constraints on the origin of continental alkalic and tholeiitic basalt, Chem. Geol. 88 (1990) 1–33.

[27] X. Xu, S.Y. O'Reilly, W.L. Griffin, The nature of the Cenozoic lithosphere at Nushan, eastern China, Geodyn. Ser. 27 (1998) 167–196.

[28] X. Xu, S.Y. O'Reilly, W.L. Griffin, X. Zhou, Genesis of young lithospheric mantle in Southeastern China: an LAM-ICPMS trace element study, J. Petrol. 41 (2000) 111–148.

[29] X. Xu, Thermo-tectonic destruction of the Archean lithosphere keel beneath the Sino–Korean Craton in China: evidence, timing and mechanism, Phys. Chem. Earth, A 26 (2001) 747–757.

[30] G. Chen, Z. Song, C. An, Three dimensional crust and upper mantle structure of the North China region, Acta Geophys. Sin. 34 (1991) 172–181 (in Chinese).

[31] M.A. Menzies, W. Fan, M. Zhang, Palaeozoic and Cenozoic lithoprobes and the loss of > 120 km of Archean lithosphere, Sino–Korean craton, China, in: H.M. Prichard, T. Alabaster, N.B.W Harris, C.R. Neary (Eds.), Magmatic processes and plate tectonics, Spec. Publ.-Geol. Soc. Lond., vol. 76, 1993, pp. 71–81.

[32] J. Deng, H. Zhao, Z. Luo, Z. Guo, X. Mo, Mantle plumes and lithosphere motion in east Asia, Geodyn. Ser. 27 (1998) 59–66.

[33] J. Deng, X. Mo, H. Zhao, A new model for the dynamic evolution of Chinese lithosphere: continental root plume tectonics, Earth Sci. Rev. 65 (2004) 223–275.

[34] J. Zheng, S.Y. O'Reilly, W.L. Griffin, F. Lu, M. Zhang, N.J. Pearson, Relict refractory mantle beneath the eastern North China block: significance for lithospheric evolution, Lithos 57 (2001) 43–66.

[35] S. Gao, R.L. Rudnick, R.W. Carlson, W.F. McDonough, Y.S. Liu, Re–Os evidence for replacement of ancient mantle lithosphere beneath the North China Craton, Earth Planet. Sci. Lett. 198 (2002) 307–322.

[36] H. Zhang, J. Zheng, Geochemical characteristics and petrogenesis of Mesozoic basalts, northeastern China: a case study of Fuxin, Liaoning, Chin. Sci. Bull. 48 (2003) 924–930.

[37] J. Yan, J. Chen, Z. Xie, Mantle xenoliths in Late Cretaceous basalts in eastern Shandong: new constraints on the timing of eastern China lithospheric thinning, Chin. Sci. Bull. 8 (2003) 1570–1574.

[38] F. Wang, H. He, R. Zhu, H. Sang, Y. Wang, L. Yang, Intercalibration of international and domestic $^{40}Ar/^{39}Ar$ dating standards, Sci. China (D) 49 (2006) 461–470.

[39] M. Flisch, Potassium–argon analysis, in: G.S. Odin (Ed.), Numerical Dating in Stratigraphy, Wiley, Chichester, 1982, pp. 151–158.

[40] T.L. Spell, I. McDougall, Characterization and calibration of $^{40}Ar/^{39}Ar$ dating standards, Chem. Geol. 198 (2003) 189–211.

[41] P.R. Renne, C.C. Swisher, A.L. Deino, D.B. Karner, T.L. Owens, D.J. Depaolo, Intercalibration of standards, absolute ages and uncertainties in $^{40}Ar/^{39}Ar$ dating, Chem. Geol. 145 (1998) 117–152.

[42] H.Y. He, X.L. Wang, Z.H. Zhou, F. Wang, R.X. Zhu, Timing of the Jiufotang formation (Jehol Group) in Liaoning northeastern China, and its implications, Geophys. Res. Lett. 31 (2004) L12605, doi: 10.1029/2004GL019790.

[43] J.R. Taylor, An Introduction to Error Analysis: The Study of Uncertainties in Physical Measurements, Univ. Sci. Books, Mill Valley, Calif., 1982, 270 pp.

[44] D. York, Least squares fitting of a straight line with correlated errors, Earth Planet. Sci. Lett. 5 (1969) 320–324.

[45] F. Begemann, K.R. Ludwig, G.W. Lugmair, K. Min, L.E. Nyquist, P.J. Patchett, P.R. Renne, C.Y. Shih, I.M. Villa, R.J. Walker, Call for an improved set of decay constants for geochronological use, Geochim. Cosmochim. Acta 65 (2001) 111–121.

[46] C.H. Lo, T.C. Onstott, C.H. Chen, T. Lee, An assessment of $^{40}Ar/^{39}Ar$ dating of the whole-rock volcanic samples from the Luzon Arc near Taiwan, Chem. Geol. 114 (1994) 157–178.

[47] A.A.P. Koppers, H. Staudigel, J.R. Wijbrans, Dating crystalline groundmass separates of altered Cretaceous seamount basalts by the $^{40}Ar/^{39}Ar$ incremental heating technique, Chem. Geol. 166 (2000) 139–158.

[48] A.A.P. Koppers, H. Staudigel, Hugh-resolution $^{40}Ar/^{39}Ar$ dating of the oldest oceanic basement basalts in the western Pacific basin, Geochem. Geophys. Geosyst. 4 (11) (2003) 8914, doi: 10.1029/2003GC000574.

[49] T.M. Harrison, I. McDougall, Excess 40Ar in metamorphic rocks from Broken Hill, New South Wales: implications for $^{40}Ar/^{39}Ar$ age spectra and the thermal history of the region, Earth Planet. Sci. Lett. 55 (1981) 123–149.

[50] S. Claesson, J.C. Roddick, $^{40}Ar/^{39}Ar$ data on the age and metamorphism of the Ottfjället dolerites, Särv Nappe, Swedish Caledonides, Lithos 16 (1983) 61–73.

[51] J. Shao, L. Zhang, B. Mu, Thermo-tectonic evolution in middle and south part of Dahinggan, Sci. China, Ser. D 28 (1998) 194–200.

[52] G.A. Davis, Y. Zheng, C. Wang, B.J. Darby, C. Zhang, G. Gehrels, Mesozoic tectonic evolution of the Yanshan fold and thrust belt, with emphasis on Hebei and Liaoning provinces, Northern China, in: M.S. Hendrix, G.A. Davis (Eds.), Paleozoic and Mesozoic tectonic Evolution of Central Asia: from continental assembly to intracontinental deformation, Geol. Soc. Am. Mem., vol.194, 2001, pp. 171–198.

[53] P.E. Smith, N.M. Evensen, D. York, M.M. Chang, F. Jian, J.L. Li, S. Cumbaa, D. Russell, Dates and rates in ancient lakes: 40Ar–39Ar evidence for an Early Cretaceous age for the Jehol Group, northeastern China, Can. J. Earth Sci. 32 (1995) 1426–1431.

[54] C.C. Swisher III, Y.Q. Wang, X.L. Wang, X. Xu, Y. Wang, Cretaceous age for the feathered dinosaurs of Liaoning, China, Nature 400 (1999) 58–61.

[55] Z. Luo, L. Miao, K. Guan, Y. Qiu, Y. Qiu, N.J. McNaughton, D.I. Groves, SHRIMP U–Pb zircon age of magmatic rock in Paishanlou gold mine district, Fuxin, Liaoning Province, China, Geochimica 30 (2001) 483–490 (in Chinese with English abstract).

[56] L. Miao, Temporal and spatial evolution of granitoids in the northern marginal zone of the North China Craton and their relationships to gold mineralization, Doctoral Dissertation, China University of Geosciences, 2002, 126 pp.

[57] Y. Chen, W. Chen, Mesozoic Volcanic Rocks: Chronology, Geochemistry and Tectonic Background, Seismology Press, Beijing, 1997, 279 pp.

[58] Y. Liu, P. Li, S. Tian, SHRIMP U–Pb zircon age of Late Mesozoic tuff (lava) in Luanping basin, northern Hebei, and its implication, Acta Petrol. Mineral. 22 (2003) 237–244 (in Chinese with English abstract).

[59] Y. Li, M. Zhai, J. Yang, L. Miao, H. Guan, Gold mineralization age of the Anjiayingzi gold deposit in Chifeng county, inner Mongolia and implications for Mesozoic metallogenic explosion in North China, Sci. China (D) 47 (2004) 115–121.

[60] S. Wang, Y. Wang, H. Hu, Z. Zhang, The existing time of Siheton vertebrate in western Liaoning' China: evidence from U–Pb age of zircon, Chin. Sci. Bull. 46 (2001) 779–782.

[61] R.X. Zhu, C. Lo, R. Shi, Y. Pan, G. Shi, J. Shao, Is there a precursor to the Cretaceous normal superchron? New paleointensity and age determination form Liaoning province, northeastern China, Phys. Earth Planet. Interior. 147 (2004) 117–126.

[62] R.X. Zhu, K.A. Hoffman, S. Nomada, P.R. Renne, R. Shi, Y. Pan, G. Shi, Geomagnetic paleointensity and direct age determination of the ISEA (M0r?) chron, Earth Sci. Planet. Lett. 217 (2004) 285–295.

[63] H.Y. He, X.L. Wang, F. Jin, Z.H. Zhou, F. Wang, L.K. Yang, X. Ding, A. Boven, R.X. Zhu, $^{40}Ar/^{39}Ar$ dating of the Early Jehol Biota from Fengning, Hebei Province, northern China, Geochem. Geophys. Geosyst. 7 (2006) Q04001, doi: 10.1029/2005GC001083.

[64] D. Wang, Volcanic rocks of Mesozoic–Cenozoic rifting in eastern China, Bull. Changchun Coll. Geol. 3 (1986) 18–32 (in Chinese).

[65] H. Zhao, J. Deng, F. Chen, 1994, Characteristics of Mesozoic volcanic rocks and their geological setting on southeast of Songliao Basin, Continental Tectonic Scientific Symposium Abstract, Beijing, 101 (in Chinese).

[66] F. Lu, Q. Zhu, S. Li, Y. Xie, J. Zheng, Mesozoic volcanism surrounding Songliao Basin, China: implication for the relationship with evolution of basin, J. China Univ. Geosci. 8 (1997) 72–77.

[67] W. Liu, W. Siebel, X. Li, X. Pan, Petrogenesis of the Linxi granitoids, northern inner Mongolia of China: constraints on basaltic underplating, Chem. Geol. 219 (2005) 5–35.

[68] B.M. Jahn, F. Wu, R. Capdevila, S. Fourcade, Y. Wang, Z. Zhao, Highly evolved juvenile granites with tetrad REE patterns: the Woduhe and Baerzhe granites from the Great Xing'an (Khingan) Mountains in NE China, Lithos 59 (2001) 171–198.

[69] F. Wu, D.Y. Sun, H.M. Li, B.M. Jahn, S.A. Wilde, A-type granites in Northeastern China: age and geochemical constraints on their petrogenesis, Chem. Geol. 187 (2002) 143–173.

[70] M. Grant, S.A. Wilde, F.Y. Wu, J.W. Valley, M.J. Spicuzza, Y.J. Chen, 2003, Emplacement of low $\delta^{18}O$ A-type granitoids in northeastern China during the Early Cretaceous. The Origin of granites and related rocks (Abstract of Hutton Symposium V), 36.

[71] J. Ying, X. Zhou, H. Zhang, Geochemical and isotopic investigation of the Laiwu–Zibo carbonatites from western Shandong Province, China, and implications for their petrogenesis and enriched mantle source, Lithos 75 (2004) 413–426.

[72] J. Shao, L. Zhang, Mesozoic dyke swarms in the north of Northern China, Acta Petrol. Sin. 18 (2002) 312–318 (in Chinese with English abstract).

[73] Y. Zheng, S. Wang, Y. Wang, An enormous thrust nappe and extensional metamorphic complex newly discovered in Sino–Mongolian boundary area, Sci. China 34 (1991) 1145–1152.

[74] L.E. Webb, S.A. Graham, C.L. Johnson, G. Badarch, M.S. Hendrix, Occurrence, age, and implications of the Yagan–Onch Hayrhan metamorphic core complex, southern Mongolia, Geology 27 (1999) 143–146.

[75] P.A. Van der Beek, D. Delvaux, P.A.M. Adriessen, K.G. Levi, Early Cretaceous denudation related to convergent tectonics in the Baikal region, SE Siberia, J. Geol. Soc. (Lond.) 153 (1996) 513–515.

[76] Y.A. Zorin, Geodynamics of the western part of the Mongol–Okhotsk collisional belt, Trans–Baikal region (Russia) and Mongolia, Tectonophysics 306 (1999) 33–56.

[77] L.A. Kozubova, S.L. Mirkina, G.A. Murina, Y.P. Shergina, A.G. Rublev, G.V. Alexandrov, Polychronous high-grade metamorphism in active zones of the Trans–Baikal region, Izv. Akad. Nauk, Ser. Geol. 12 (1980) 22–33.

[78] I.G. Rutshtein (Ed.), 1992, Geological Map of the Chita region (1:500,000). MPGIT, Moscow, 23 sheets.

[79] X. Zhang, T. Li, Z. Pu, 40Ar–39Ar thermochronology of two ductile shear zone from Yiwulüshan, West Liaoning Region: age constraints on the Mesozoic tectonic events, Chin. Sci. Bull. 47 (2002) 1113–1118.

[80] X. Zhang, T. Li, Z. Pu, H. Wang, ^{40}Ar–^{39}Ar ages of Louzidian–Dachengzi ductile shear zone near Chifeng, Inner Mongolia and their tectonic significance, Chin. Sci. Bull. 47 (2002) 1292–1297.

[81] M.A. Menzies, Y. Xu, Geodynamics of the North China Craton, in: M.F.J. Flower, S.L. Chung, C.H. Lo, T.Y. Lee (Eds.), Mantle dynamics and plate interactions in East Asia, Am Geophy. Union, Washington, D. C., Geodyn. Ser., vol. 100, 1998, pp. 155–165.

[82] F. Wu, R.J. Walker, X.W. Ren, D.Y. Sun, X.H. Zhou, Osmium isotopic constraints on the age of lithospheric mantle beneath northeastern China, Chem. Geol. 197 (2003) 107–129.

[83] M.P. Watson, A.B. Hayward, D.N. Parkinson, Z.M. Zhang, Plate tectonic history, basin development and petroleum source rock deposition onshore China, Mar. Pet. Geol. 4 (1987) 205–225.

[84] J.J. Traynor, C. Sladen, Tectonic and stratigraphic evolution of the Mongolian People's Republic and its influence on hydrocarbon geology and potential, Mar. Pet. Geol. 12 (1995) 35–52.

[85] L. Ratschbacher, B.R. Hacker, L.E. Webb, M. McWilliams, T. Ireland, S.W. Dong, A. Calvert, D. Chateigner, H.R. Wenk, Exhumation of the ultrahigh-pressure continental crust in east central China: Cretaceous and Cenozoic unroofing and the Tan–Lu fault, J. Geophys. Res. 105 (2000) 13303–13338.

[86] P. Castillo, The duple anomaly as a trace of upwelling lower mantle, Nature 336 (1988) 667–670.

[87] R.A. Duncan, M.A. Richards, Hotspots, mantle plume, flood basalts and true polar wander, Rev. Geophys. 29 (1991) 31–50.

[88] B.R. Hacker, L. Ratschbacher, L. Webb, T. Ireland, D. Walker, S.W. Dong, U/Pb zircon ages constrain the architecture of the ultrahigh-pressure Qinling–Dabie Orogen, China. Earth Planet, Sci. Lett. 161 (1998) 215–230.

[89] B. Chen, B.M. Jahn, Y. Arakawa, M.G. Zhai, Petrogenesis of the Mesozoic intrusive complexes from the southern Taihang Orogen, North China Craton: elemental and Sr–Nd–Pb isotopic constraints, Contrib. Mineral. Petrol. 148 (2004) 489–501.

[90] X.H. Li, Cretaceous magmatism and lithospheric extension in southeast China, J. Asian Earth Sci. 18 (2000) 293–305.

[91] P. Machetel, E. Humler, High temperature during Cretaceous avalanche, Earth Planet. Sci. Lett. 208 (2003) 125–133.

[92] S.A. Wilde, X.H. Zhou, A.A. Nemchin, M. Sun, Mesozoic crust-mantle beneath the North China craton: a consequence of the dispersal of Gondwana land and accretion of Asia, Geology 31 (2003) 817–820.

[93] R.L. Larson, Latest pulse of Earth: evidence for a mid-Cretaceous superplume, Geology 19 (1991) 547–550.

[94] P. Bird, Continental delamination and the Colorado Plateau, J. Geophys. Res. 84 (1979) 7561–7571.

[95] S.P. Turner, J.P. Platt, R.M.M. George, S.P. Kelley, D.G. Pearson, G.M. Nowell, Magmatism association with orogenic collapse of the Betic–Alboran Domain, SE Spain, J. Petrol. 40 (1999) 1011–1036.

[96] J. Shao, B. Mu, L. Zhang, Deep geological process and its shallow response during Mesozoic transfer of tectonic framework in eastern North China, Geol. Rev. 46 (2000) 32–40 (in Chinese with English abstract).

[97] Q. Fan, R. Liu, H. Li, N. Li, J. Sui, Z. Lin, Zircon chronology and REE Geochemistry of granulite xenoliths at Hannuoba, Chin. Sci. Bull. 43 (1998) 1510–1515.

[98] Y. Liu, S. Gao, H. Yuan, L. Zhou, X. Liu, X. Wang, Z. Hu, L. Wang, U–Pb zircon ages and Nd, Sr, and Pb isotopes of lower crustal xenoliths from North China: insights on evolution of lower continental crust, Chem. Geol. 211 (2004) 87–109.

[99] M. Zhai, R. Zhu, J. Liu, Q. Meng, Q. Hou, S. Hu, Z. Li, H. Zhang, W. Liu, Time range of Mesozoic tectonic regime inversion in eastern North China Block, Sci. China, Ser. D 47 (2004) 151–159.

[100] J. Ren, K. Tamaki, S. Li, J. Zhang, Late Mesozoic and Cretaceous rifting and its dynamic setting in Eastern China and adjacent areas, Tectonophysics 344 (2002) 175–205.